STUDY OF TEMPORAL MICROCLIMATIC VARIABILITY AND ITS IMPACT ON SOYBEAN (*GLYCINE MAX* (L.) MERRILL) DEVELOPMENT IN A PROTECTED ENVIRONMENT: A PRECISION AGRICULTURE APPROACH.

João Guilherme Risardi[1], Paulo Sergio de Paula Herrmann Junior[2],

André Torre Neto[3] and Paulo Estevão Cruvinel[4]

[1]Mechanical Engineer and M.Sc. student in Computer Science, Embrapa Instrumentation and Federal University of São Carlos (UFSCar), Brazil
[2]Doctor in Physical Chemistry, Senior Researcher, Embrapa Instrumentation, Brazil
[3]Doctor in Applied Physics, Senior researcher, Embrapa Instrumentation, Brazil
[4]Doctor in Automation, Senior Researcher, Embrapa Instrumentation and Postgraduate Program in Computer Science, Federal University of São Carlos (UFSCar), Brazil

Corresponding authors: joaoguilherme.risardi@colaborador.embrapa.br (Risardi, J.G.[1]), paulo.herrmann@embrapa.br (Herrmann Junior, P.S.P.[2]), andre.torre@embrapa.br (Torre Neto, A.[3]), paulo.cruvinel@embrapa.br (Cruvinel, P.E.[4])

A paper from the Proceedings of the
17th International Conference on Precision Agriculture and 11th Brazilian Congress on Precision and Digital Agriculture
13-15 July 2026
Porto Alegre, Brazil

Abstract.

Soybean, belonging to the Fabaceae family, is a leguminous crop of high economic and nutritional value, widely cultivated in Brazil, which ranks among the world's largest producers and exporters. However, the growing demand for productivity has driven the adoption of digital technologies and Precision Agriculture (PA) methods aimed at intelligent crop management. In protected environments, cultivation allows the mitigation of external constraints, although it does not eliminate internal thermal and moisture variations that may influence plant growth and photosynthetic efficiency. In this context, understanding the vegetative stage of soybean is crucial to defining its productive potential. The V1 to V5 period (from the first trifoliate leaf to the fifth node with open trifoliates) usually occurs between 10 and 30 days after emergence, depending on the cultivar, temperature, relative humidity, and carbon dioxide (CO_2) concentration. For seedlings to develop vigorous shoots, roots, and nodules, it is essential to monitor microclimatic conditions within predefined risk ranges for management actions. Thus, temperature (°C) is considered low risk between 20–32°C, medium risk between 10–20°C, and high risk below 10°C or above 35°C, which causes protein degradation and impairs photosynthesis; relative humidity (%) is low risk between 60–80%, medium between 40–60%, and high below 40% or above 85%, which favors

The authors are solely responsible for the content of this paper, which is not a refereed publication. Citation of this work should state that it is from the Proceedings of the 17th International Conference on Precision Agriculture and 11th Brazilian Congress on Precision and Digital Agriculture. Risardi, J.G., Herrmann Junior, P.S.P., Torre Neto, A., Cruvinel, P.E. (2026). Study of temporal microclimatic variability and its impact on soybean (*Glycine max* (L.) Merrill) development in a protected environment: a precision agriculture approach. In Proceedings of the 17th International Conference on Precision Agriculture and 11th Brazilian Congress on Precision and Digital Agriculture (unpaginated, online). Monticello, IL: International Society of Precision Agriculture and Brazilian Congress on Precision and Digital Agriculture.

fungal incidence; and CO_2 concentration (ppm) is low risk above 450 ppm, medium between 300–450 ppm, and high below 300 ppm, compromising photosynthetic capacity. The study aimed to analyze the temporal variability of microclimatic variables and their relationship with soybean vegetative development. Experiments were conducted using the BR-16 cultivar at Embrapa Instrumentation (São Carlos, SP, 22°00'45.3"S 47°53'46.4"W) into a semi-controlled polymethyl methacrylate chamber® designed for continuous microclimatic monitoring and gas sampling. The structure, installed in an indoor environment, allows light and solar radiation to enter. Sensors used included a Vaisala GMP222 (CO_2), a digital semiconductor sensor (temperature), and a capacitive sensor (relative humidity), recording measurements every five minutes over 56 consecutive days. Time series were processed in Python, including outlier treatment, decomposition of trend, seasonality, and noise components, as well as the application of moving windows of 3 and 5 days, corresponding to the average transition time between phenological stages. This approach enabled the analysis of the non-stationary behavior of the variables, identification of oscillation patterns, and delineation of low-, medium-, and high-risk ranges for vegetative development under varying microclimatic conditions. The analyses revealed marked diurnal cycles, alternating periods of thermal and moisture instability with windows of microclimatic equilibrium. As cultivation was carried out in a protected environment, the occurrence of the aforementioned risk conditions was confirmed, although with a predominance of microclimatic windows associated with medium and high risks. The results demonstrate that monitoring temporal microclimatic variability, integrated with the soybean vegetative stage, constitutes an effective Precision Agriculture technique. This approach showed high diagnostic value, providing decision support for the improvement of crop management and the potential mitigation of production risks.

Keywords.

Precision Agriculture, Temporal Variability, Microclimate, Phenotyping, Soybean.

1. Introduction

Precision Agriculture (PA) has established itself as a relevant approach to capturing the spatial and temporal variability of agricultural systems, enabling continuous monitoring of environmental variables and a more efficient use of resources (Silva and Mann 2023). PA utilizes technologies such as sensors and the Internet of Things (IoT) to monitor these variations. Kagan et al. (2022) report that IoT-based systems are revolutionizing agricultural practices by enabling microclimate capture and the early identification of biotic and abiotic stresses across spatial, temporal, and compositional dimensions.

In this scenario, time-series analysis methods emerge as tools capable of understanding the dynamics of these variables over time, allowing the identification of relevant patterns, trends, and extreme events often missed by spatial approaches. Globally, this analytical approach based on high-resolution temporal data finds a critical field of application in the monitoring of soybean *Glycine max* (L.) Merrill. In the case of Brazil, this aspect gains even greater importance, given that the soybean crop is consolidated as one of the country's primary agricultural commodities.

Soybean, belonging to the Fabaceae (legume) family, is an annual herbaceous plant widely used as a source of protein and oil for human and animal nutrition. Brazil stands out as the world's largest producer and exporter of this oilseed, reaching a production of 180.13 million metric tons in a planted area of 48.72 million hectares in the 2025/26 crop year (Embrapa Soja 2026). The growing demand for yield has driven the evolution of technologies aimed at the efficient and sustainable management of the crop. In light of this, the global economic relevance of soybean can be observed by the continuous growth of national production in recent decades (Figure 1).

Soybean development is strongly influenced by environmental conditions, such that variables such as air temperature and relative humidity directly affect the crop's transpiration rate and biomass accumulation (Zhang et al. 1995; Jumrani et al. 2022). Additionally, the dynamics of CO_2 concentration act as an essential modulating factor in photosynthesis processes and stomatal efficiency (He and Matthews 2023). Therefore, understanding microclimatic interactions throughout the plant phenological cycle requires the use of structures for monitoring variables, such as automated growth chambers, which minimize the interference of external factors and enable high temporal resolution analysis (Herrmann et al. 2024).

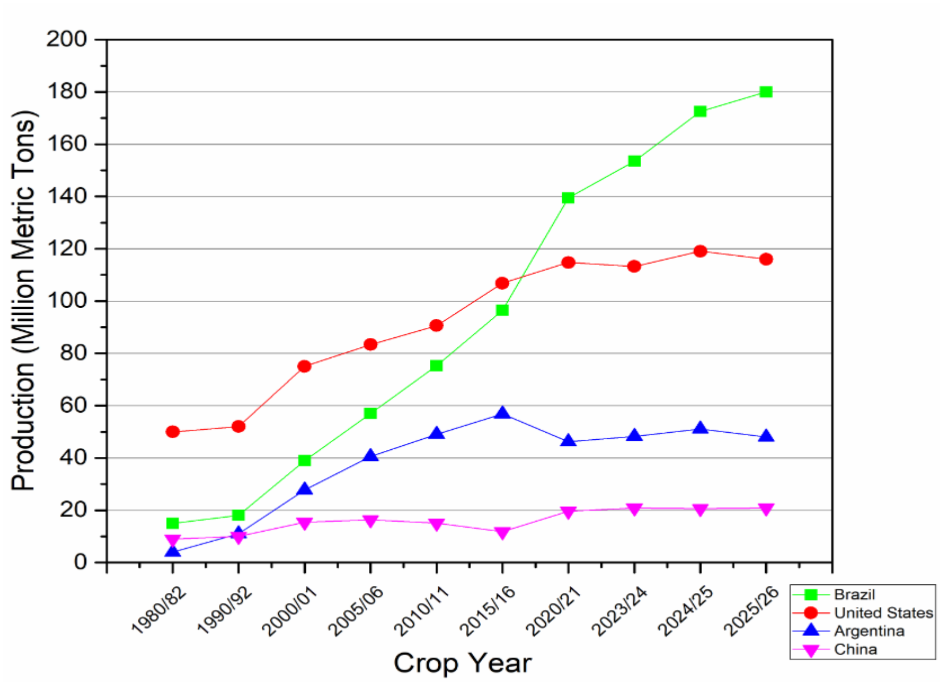

Fig. 1. Harvests related to the world's main soybean-producing countries per year (in million metric tons); forecasts through April 2026 (Source: Adapted from United States Department of Agriculture, 2026).

However, even in these protected systems, the behavior of microclimatic variables is not static. Temporal fluctuations in temperature and relative humidity still occur due to solar radiation, thermal exchange with the environment, and low (or absent) natural ventilation. These oscillations can affect fundamental physiological processes, such as transpiration, photosynthesis, and plant water balance (Kronenberg et al. 2020).

The thermal and moisture behaviors in these systems exhibit characteristic dynamics over time. During the daytime, the incidence of solar radiation promotes heat accumulation, raising the internal temperature and reducing relative humidity. Conversely, during the nighttime, temperature decreases and relative humidity increases, potentially reaching levels close to saturation. These oscillations configure a dynamic regime that can expose plants to stress conditions, especially when extreme values are reached or maintained for prolonged periods (Farias et al. 2007).

Despite advances in environmental monitoring within protected environments, most studies focus on spatial analysis of variables or punctual evaluations. There remains, therefore, a gap in the literature regarding the periodic temporal dynamics of these variables and how they impact the crop throughout the vegetative development cycle, specifically from phenological stages V1 to V5. Evaluating the temporal variability of these target variables is fundamental to addressing the ongoing challenges of precision agriculture.

Previous studies, such as that by Herrmann et al. (2024), demonstrated the potential of integrating environmental sensors and an electronic nose (E-nose) for high-throughput plant phenotyping applications. Although that study only addressed the integration of environmental variables and chemical signals detected by the electronic nose for phenotyping, it opened an opportunity to thoroughly explore the temporal variability of the microclimate and its impact on crop development.

Furthermore, few studies address microclimatic variability from the perspective of plant phenological stages—particularly vegetative stages, which are decisive for expanding productive capacity. Specifically, the V5 stage is a critical phase for boosting soybean yield potential, as it defines the potential number of nodes the main stem will produce, and each node is responsible for developing lateral branches where pods will form (Endres and Kandel 2025).

Given this context, this paper presents a study on the temporal variability of microclimatic variables (temperature (°C), relative air humidity (%), and CO_2 concentration (ppm)) within a protected environment established to evaluate soybean plant development, with special attention to stages V1 to V5. Additionally, it considers the development of a microclimatic risk classification model for soybean growth.

Following this introduction, Section 2 presents the materials and methods, the materials employed, the collected data, the methodological workflow, the description and preparation of the experiment for method validation, and the analysis procedures. Section 3 presents the results and discussion. Finally, Section 4 delivers the conclusions of the study and proposes directions for future work.

2. Materials and Methods

The materials utilized in this study comprised data time series, a semi-controlled instrumented chamber for housing the target soybean plants, two soybean plants, and a computational infrastructure for data processing and results evaluation. Figure 2 illustrates a block diagram of the structured framework developed to conduct the experiments and evaluate microclimatic variability and its impact on the V5 vegetative stage of the crop.

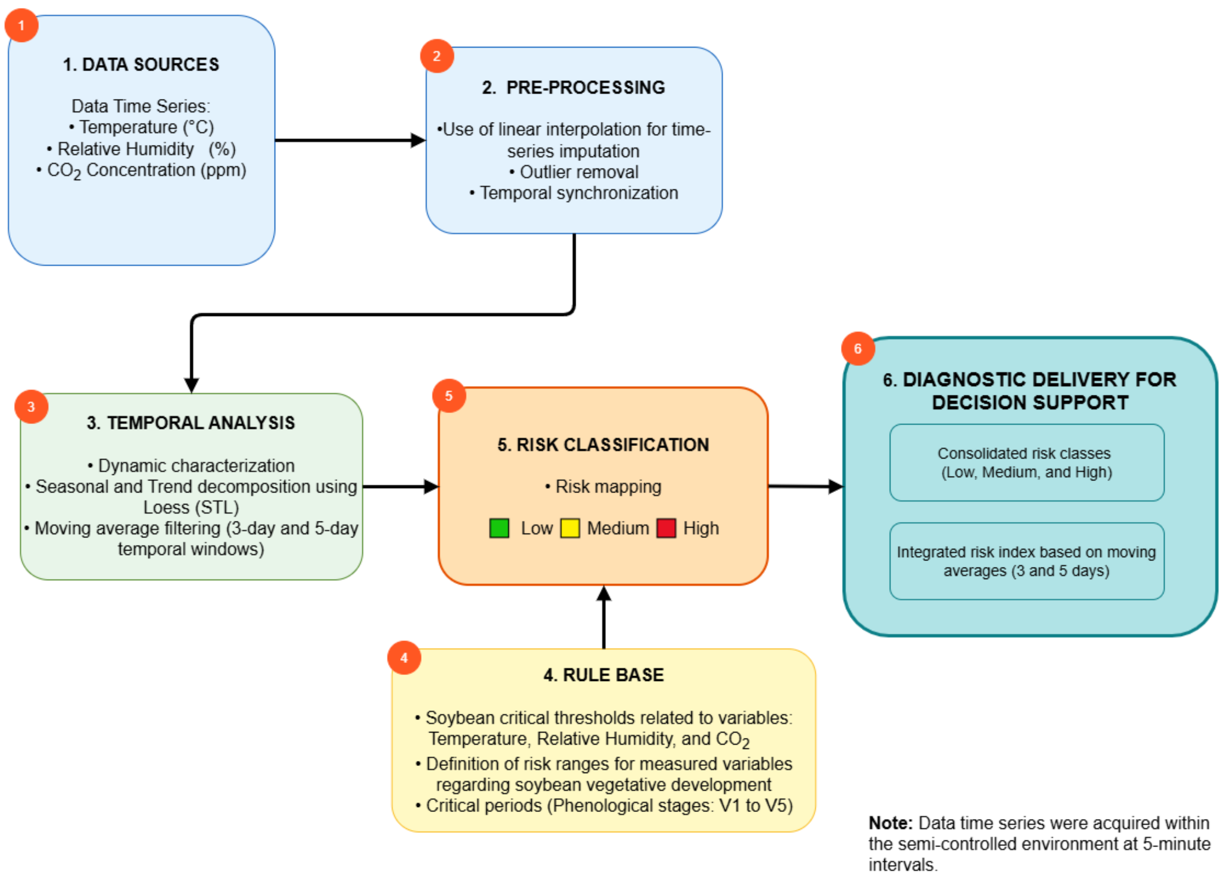

Fig. 2. Conceptual diagram of the data processing and microclimatic risk classification pipeline.

The data time series consist of records of air temperature, relative air humidity, and CO_2 concentration. Using these data, time-series analysis methods were applied to characterize the dynamics of the microclimatic variables and classify risk conditions for soybean crop development. The microclimatic risk classification was established based on the literature, considering three risk levels: low, medium, and high.

The methodological workflow encompasses the time-series processing steps, alongside a critical evaluation of aspects related to the temporal variability observed in the temperature, relative humidity, and CO_2 concentration readings, and their impact on soybean development. Particular emphasis is placed on the effects during the V5 stage of the soybean crop (Fehr and Caviness 1977), which represents a crucial vegetative phase characterized by five nodes on the main stem, four to five fully unrolled trifoliate leaves, and the latest trifoliate leaf beginning to separate. At this specific developmental juncture, the crop determines its maximum potential for branching and productive nodes (Endres and Kandel 2025).

2.1. Materials

The experiment was conducted in a semi-controlled growth chamber installed at Embrapa Instrumentação, in the city of São Carlos, São Paulo, Brazil (22°00'45.3"S, 47°53'46.4"W). The structure was designed to monitor microclimatic variables (temperature, relative air humidity, and CO_2 concentration).

The acquisition of these data resulted in the organization of time series comprising approximately 13,600 records for each monitored variable. Each dataset was structured as a univariate time series, as expressed in Equation (1):

$$Y = \{y_n | t = 1,2, \dots, n\} \tag{1}$$

where y_n represents the observed value of the variable at time t. The complete structured dataset occupies 4.2 MB of disk space and is stored in comma-separated values (CSV) file format.

The time series were processed in a Python environment using the pandas, numpy, and statsmodels libraries. Initially, data pre-processing was performed, including temporal standardization, removal of redundant attributes, missing value imputation, and identification of instrumental inconsistencies (outliers).

During the cleaning stage, redundant temporal indexing attributes and variables without operational information were eliminated, ensuring consistency and unified indexing of the series by date_time. Each record consists of the measured variable value and the identification of the source sensor. This organization enables both independent and integrated analyses of the microclimatic variables under consideration.

The chamber was positioned in an open, isolated area under direct solar radiation and instrumented for internal monitoring. The main body of the structure was fabricated from a poly(methyl methacrylate) (PMMA) tube with an outer diameter of 260 mm, an inner diameter of 250 mm, a wall thickness of 10 mm, and a total height of 570 mm, resulting in an internal volume of 27.93 L, as described by Herrmann et al. (2024). Internally, the structure features an axial fan for internal atmosphere homogenization, as well as a manual valve connected directly to the soil for irrigation with deionized water. During the experimental period, no active climate control was applied, so the observed variations reflected the natural behavior of the internal microclimate (Figure 3).

The crop utilized in this study was the Brazilian soybean cultivar BR-16, developed and released by the Brazilian Agricultural Research Corporation (Embrapa 1991).

The substrate used was a dystrophic Red-Yellow Latosol (Oxisol) (Papa et al. 2011). The soil sample was obtained from the National Precision Agriculture Laboratory (LANAPRE) at Embrapa, located at the geographical coordinates 21°57'14"S and 47°51'08"W, 860 m above sea level.

Water management and system irrigations were carried out exclusively using high-purity deionized water (Milli-Q, ~12 MΩ·cm).

For the internal monitoring of the chamber's CO_2 concentration (ppm), a Vaisala CO_2 Probe GMP222 (Vaisala Oyj, Vantaa, Finland) was installed, operating within a measurement range of 0 to 2,000 ppm, with an accuracy (at 25 °C and 1,013 hPa) of ±1.5% of the range + 2% of the reading. For relative air humidity (%) and temperature (°C) measurements, a Vaisala Humitter 50 YC sensor (Vaisala Oyj, Vantaa, Finland) was used, which features a measurement range of 0 to 100% for relative humidity, with an accuracy of ±3% in the 10% to 90% range at 20 °C, and a temperature measurement range of –10 °C to +60 °C, with an accuracy of ±0.5 °C. The output signal ranges from 0 to 1 V, corresponding to 0–100% relative humidity and –40 to +60 °C temperature.

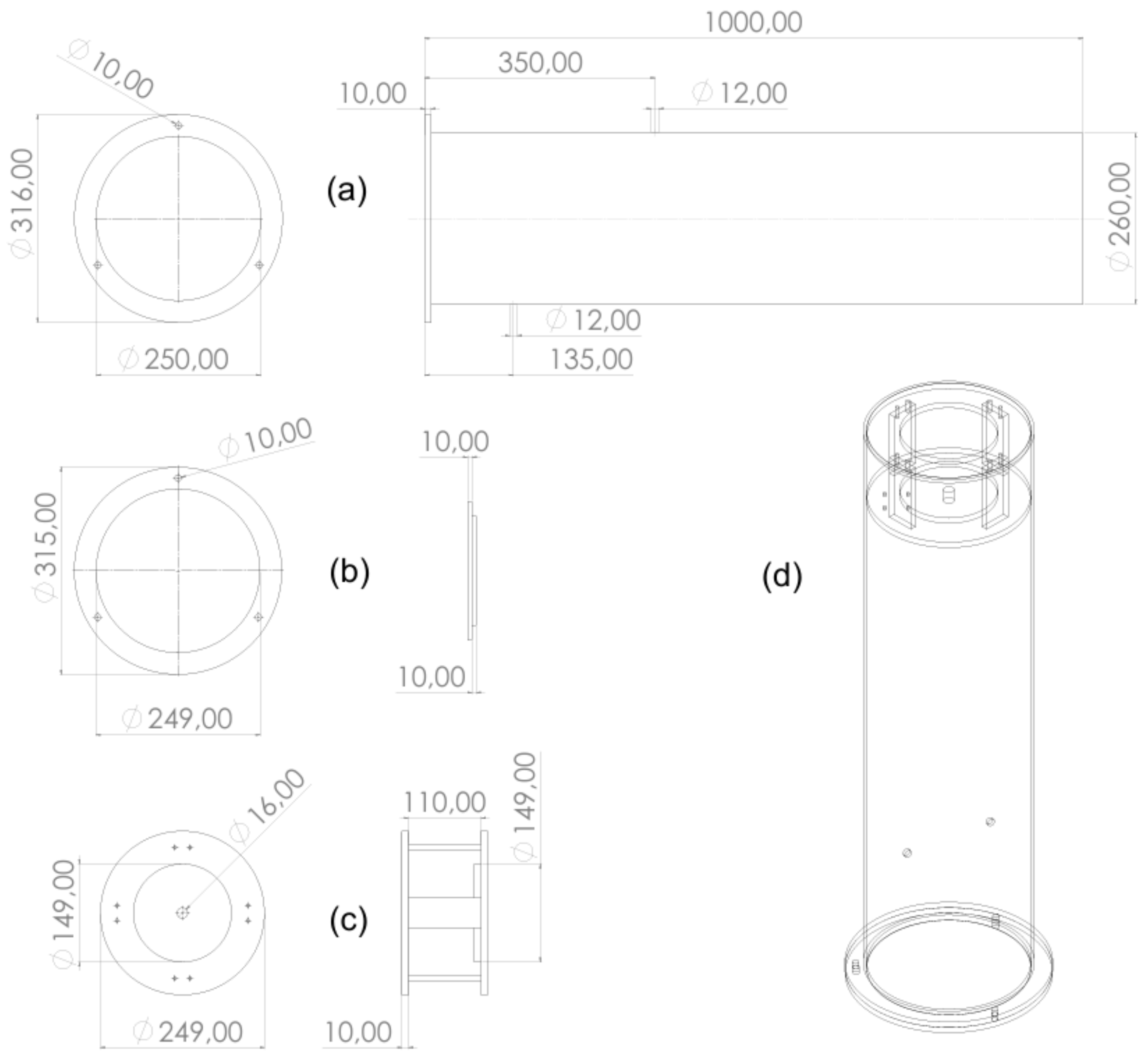

Fig. 3. Technical drawing and dimensional detailing of the structural components of the semi-controlled growth chamber®: (a) flanged structural tube; (b) base plate featuring an O-ring for bottom sealing and support feet; (c) top cover for sensor coupling, axial fan, and gas sample collector; and (d) 3D isometric view of the assembled chamber. All dimensions are in millimeters (mm) and presented at a 1:2 scale.

The processing and analysis of the time series were performed on a workstation running the Windows 11 Pro for Workstations (64-bit) operating system, located at the Precision Agricultural Applications Laboratory at Embrapa Instrumentação. The workstation is equipped with an Intel® Xeon® E-2236 CPU @ 3.40 GHz processor and 64 GB of RAM.

2.2. Methods

A volume of 100 mL of Milli-Q water was applied every two days, a management regime that was maintained until the V5 phenological stage. After this period, water supply was interrupted to induce water deficit within the semi-controlled environment. The monitoring of air temperature, relative air humidity, and CO_2 concentration was continued until plant senescence occurred. Communication was established via the Zigbee protocol (Telegesis ETRX357 module (Telegesis Ltd., London, United Kingdom), 2.4 GHz – IEEE 802.15.4), a wireless communication protocol that transmits data via radio signals (Figure 4).

Data were collected at regular five-minute intervals, generating a detailed and periodic temporal sampling of the environmental factors (temperature, relative humidity, and CO_2 concentration) inside the chamber. This information was received by a Zigbee Coordinator connected to the serial (USB) port of a computer. The data were then routed via the Node-RED™ visual programming tool to a local IoT database using InfluxDB®, an open-source database management system specialized in time series.

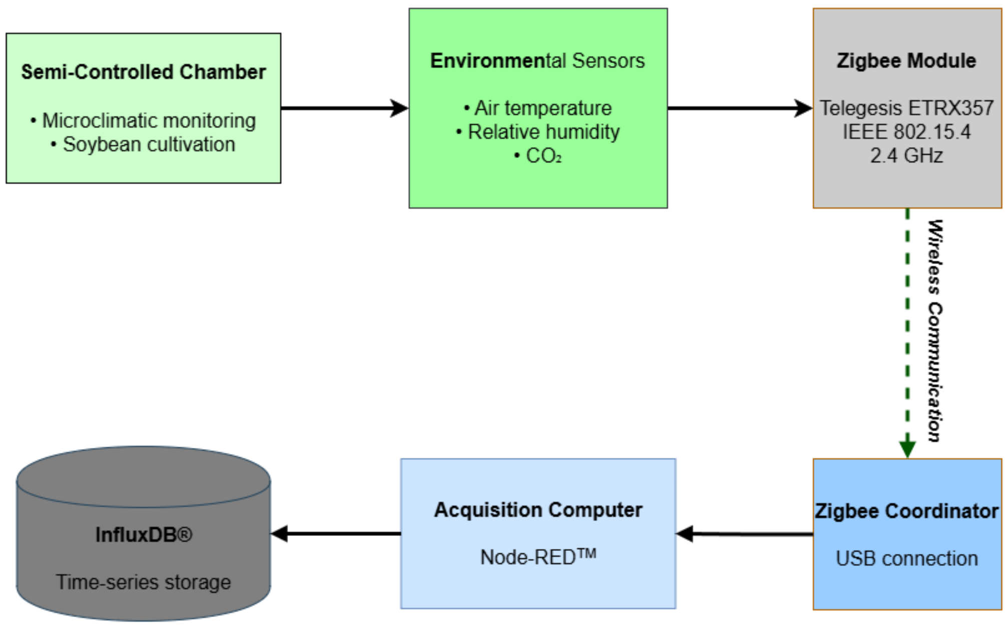

Fig. 4. Block diagram of the microclimatic data acquisition system.

Since direct morphological records of the plants (such as the number of nodes or trifoliate leaves) were not available, the V1–V5 phenological stages were temporally estimated based on the average transition interval between vegetative stages described in the literature. For this purpose, moving windows of 3 and 5 days after the onset of experimentally observed vegetative development were considered (Neumaier et al. 2000).

For the temporal variability analysis, time-series decomposition was performed using the Seasonal and Trend decomposition using Loess (STL) algorithm from the statsmodels library. This method was used to separate the time series into their trend (T_t), seasonal (S_t), and residual (R_t) components, allowing the identification of recurrent patterns and oscillations associated with the microclimatic behavior of the protected environment. To achieve this, the time series Y_t were represented according to the additive model described in Equation (2):

$$Y_t = T_t + S_t + R_t \tag{2}$$

where Y_t represents the value recorded by the sensors at time t. The trend component (T_t) reflects the long-term behavior of the series, enabling the observation of the change gradient throughout crop development. The seasonal component (S_t) represents the daily cyclic and repetitive fluctuations. Finally, R_t quantifies the residual or "noise", representing what remains after the trend and seasonality are removed.

Filtering and component estimation in STL utilize the LOESS algorithm (local polynomial regressions), allowing the seasonal component (S_t) to change dynamically in amplitude over time. Additionally, to protect against spurious readings, the robustness parameter activation criterion was utilized (robust=True). This procedure iteratively recalculates the local regression weights based on the residuals obtained in the previous iteration, directing anomalous fluctuations and outliers directly to the residual component, as expressed in Equation (3):

$$R_t = Y_t - T_t - S_t \tag{3}$$

For the temporal variability analysis and smoothing of short-term fluctuations, moving windows of size k corresponding to 3 and 5 days were applied. The moving average was calculated using Equation (4):

$$M_t = \frac{1}{k}\sum_{i=0}^{k-1} T_{t-i} \tag{4}$$

where M_t represents the smoothed value of the series at time t; k is the size of the temporal window (in this study, $k = 3$ and $k = 5$); and T_{t-i} corresponds to the previous values of the trend component obtained by STL.

For the microclimatic risk classification, air temperature, relative humidity, and CO_2 concentration variables were combined, considering optimal ranges defined in the literature for the physiological development of soybean. The objective of this approach was to identify periods of greater microclimatic stability alongside conditions potentially limiting to crop growth.

Initially, the set of three variables was verified against a rule base to establish three classification levels: low, medium, and high risk. The thresholds adopted for each variable were defined based on agronomic literature for the soybean crop, forming a rule base for the decision-support model, as presented in Table 1.

Table 1. Microclimatic risk parameters and ranges for soybean crop development.

Variable	Low Risk	Medium Risk	High Risk	Reference
Temp (°C)	20–32	10–20	<10 or >35	Farias et al. (2007)/ Jumrani et al. (2022)
RH (%)	60–80	40–60	<40 or >85	Zou and Kahnt (1988)/ He and Matthews (2023)
CO_2 (ppm)	>450	300–450	<300	Baker et al. (1989)/ Soares et al. (2021)

Thus, individual scores were assigned to satisfy Equation (5):

$$R = T + RH + CO_2 \tag{5}$$

where V_i represents the individual score of each monitored variable (T for air temperature, RH for relative air humidity, and CO_2 for carbon dioxide concentration), where 0 indicates high risk, 1 indicates medium risk, and 2 indicates low risk.

Consequently, the classification of the set of variables is represented as an integrated microclimatic risk (R), as established in Equation (6):

$$V_i = \begin{cases} 2, & if\ Low\ Risk \\ 1, & if\ Medium\ Risk \\ 0, & if\ High\ Risk \end{cases} \tag{6}$$

3. Results and Discussion

3.1. Time-Series Availability

The collected data for temperature, relative humidity, and CO_2 concentration underwent a validation process based on the operational specifications of the sensors and the physical characteristics of the experimental environment. Possible effects of thermal accumulation, local condensation, and localized gas concentrations were considered. This approach was highly relevant given that the validation experiment was conducted within a semi-controlled chamber with a volume of 27.93 L containing two developing soybean plants.

The application of a logical filter based on the operational span enabled outlier detection and removal. For temperature, values above 65 °C or below –40 °C were classified as outliers. For relative air humidity, values exceeding 100% were retained to account for potential local supersaturation and condensation near the sensor surface; values above 120% or below 0% were considered outliers. For CO_2 concentration, only negative values or those exceeding 10,000 ppm were removed, because negative values lack physicochemical meaning and values above 2,000 ppm fall outside the calibration range (Table 2).

Table 2. Physical consistency criteria and quantitative summary of invalid records removed per microclimatic variable.

Variable	Criterion	Removed Records
Temperature (°C)	>65 °C or <-40 °C	1,133
Relative Humidity (%)	>120% or <0%	1,139
CO_2 (ppm)	<0 ppm or >10000ppm	1,484

Following outlier removal, the continuity of the time series was evaluated. Short interruptions, primarily concentrated in 10-minute intervals, predominated alongside long gaps of up to 250 consecutive records (~20 h 45 min of data acquisition), which were attributed to communication and acquisition failures in the IoT system.

To correct sensor reading failures, short-duration invalid records (up to 30 minutes) were corrected via temporal linear interpolation, preventing the artificial creation of trends during prolonged periods without data acquisition. Conversely, larger gaps were maintained as missing values to preserve the original temporal structure of the series.

Regarding data completeness in the analyzed time series, the temporal coverage indicated an average availability of 87.55% of records for temperature, 87.54% for relative humidity, and 85.95% for CO_2. These percentage variations in time-series completeness resulted from both outlier elimination and instrumental failures related to the data collection processes.

3.2. Temporal Behavior of Temperature, Relative Humidity, and CO_2 Concentration

Regarding the behavior of the time series, high variability was observed across the analyzed variables, as exemplified by a subset of the results in Figure 5, characterizing a dynamic environment even under semi-controlled conditions. The analysis revealed strong, well-defined daily cyclic patterns for temperature, relative humidity, and CO_2 concentration.

The onset of the V1 phenological stage occurred on November 8, and the water supply was maintained until the V5 phenological stage (December 8), at which point water supply was interrupted to induce water deficit stress. During the regular irrigation period, temperature exhibited daily oscillations that frequently exceeded the optimal ranges for soybean development. This behavior can be attributed to thermal accumulation from solar radiation on the chamber structure, aggravated by the absence of air exchange mechanisms in the experimental chamber. Elevated temperatures reduce photosynthetic efficiency through stomatal closure and increase plant evaporative demand, thereby affecting vegetative growth and biomass accumulation.

Conversely, relative humidity remained at saturation levels, a behavior driven by plant transpiration within the sealed chamber. Although high humidity reduces water loss via transpiration, persistently saturated conditions restrict transpirational flow and can consequently halt nutrient transport, while increasing the risk of pathogen development, thus elevating the risk condition for crop development.

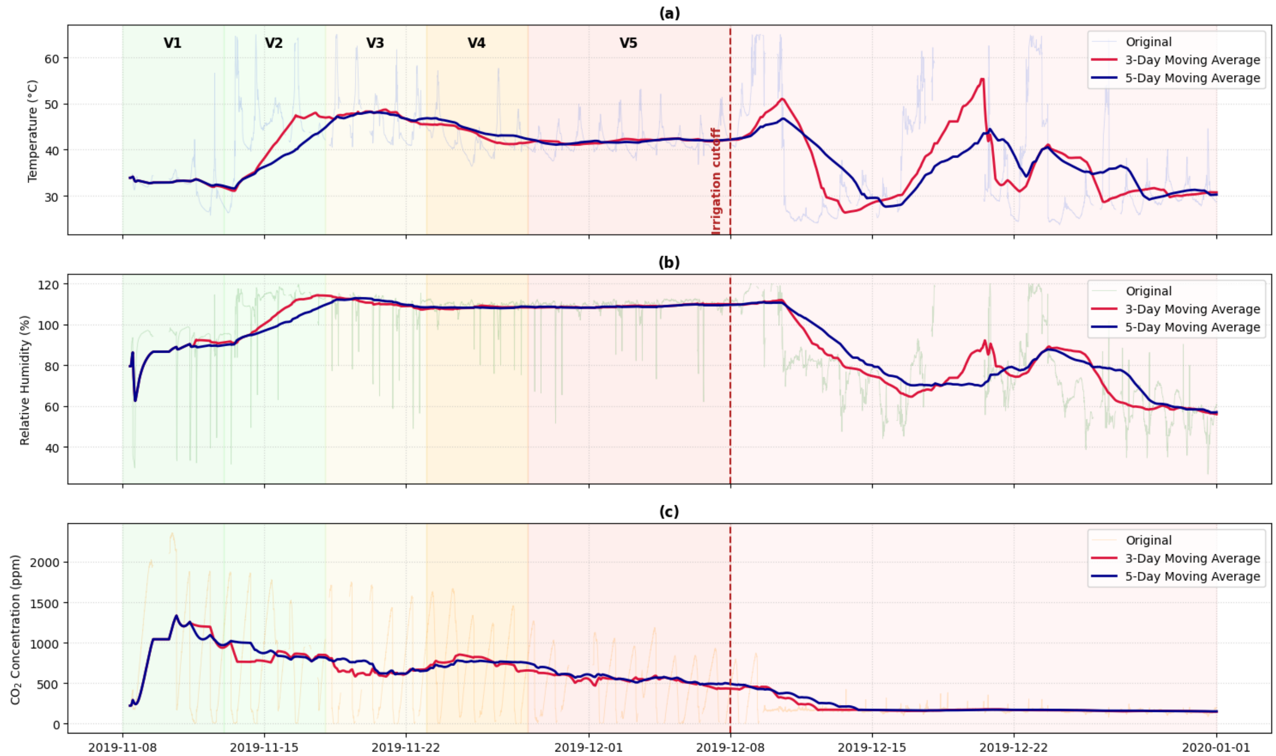

Fig. 5. Complete time series and 3- and 5-day moving averages of the microclimatic variables: (a) air temperature, (b) relative humidity, and (c) CO_2 concentration.

The application of 3- and 5-day moving averages enabled the attenuation of instrumental noise, facilitating the evaluation of impacts on transitions between the vegetative phenological stages of the target crop, with particular emphasis on phenological stages V1 to V5. These temporal windows were also utilized in the microclimatic risk assessment, assuming that unfavorable conditions maintained over prolonged periods were more likely to impact the physiological development of the crop.

Trend analysis using Seasonal and Trend decomposition using Loess (STL) enabled the independent evaluation of milestones that occurred during the experiments. One such milestone took place on December 8. On this date, the behavior of the signals showed an increase followed by a drop across all sensors (Figure 6).

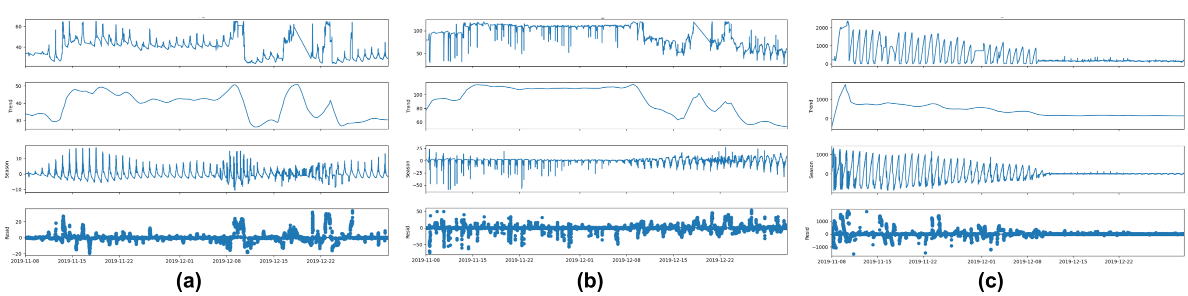

Fig. 6. Trend, seasonal, and residual components obtained via STL decomposition for: (a) air temperature, (b) relative humidity, and (c) CO_2 concentration time series.

Statistical decomposition confirmed that the transition in the hydrological regime triggered a rupture in the system equilibrium after December 8. Without water available for transpiration, the plants lost their evaporative cooling capacity, generating thermal spikes inside the structure and forcing the evaporation of residual soil moisture.

Simultaneously, the seasonal component reveals that the daily cyclic patterns between daytime photosynthetic consumption and nighttime respiratory accumulation of CO_2 gradually vanished, locking the time series into a continuous, stable line near 200 ppm. This graphical inflection marks the ecophysiological collapse of the two soybean plants allocated to the experiment, as well as the definitive breakdown of the plant-atmosphere coupling within the chamber.

These results demonstrate that, even in protected environments, the temporal variability of microclimatic conditions can generate potentially limiting situations for crop development, reinforcing the necessity of periodic monitoring of these variables under the framework of PA.

3.3. Average Hourly Profile of the Microclimate

The integration of the average hourly profile from periodic records quantified the severity limits imposed on the cultivar over a 24-hour period (Figure 7):

The average thermal profile indicated minimum temperatures of 36 °C during the early morning and average peaks of 44 °C at 1:00 PM, indicating that the semi-controlled chamber frequently operated above the ideal range for the soybean crop (Figure 7a). In contrast, relative air humidity remained continuously elevated, fluctuating around 98% in the early morning and maintaining an average minimum of 85% at 1:00 PM (Figure 7b).

Regarding CO_2 concentration, a peak accumulation occurred in the early morning hours, reaching approximately 850 ppm at 7:00 AM, followed by a severe drop induced by daytime photosynthetic consumption, which reduced gas availability to approximately 175 ppm at 4:00 PM (Figure 7c).

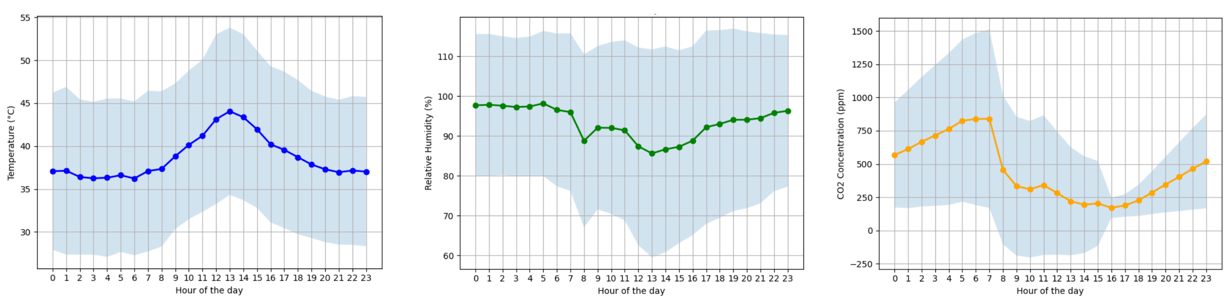

(a) (b) (c)

Fig. 7. Diurnal 24-hour microclimatic profiles within the semi-controlled growth chamber: (a) air temperature, (b) relative humidity, and (c) CO_2 concentration.

3.4. Integrated Microclimatic Risk Classification

To evaluate the combined impact of the monitored variables, the raw data were transformed into adequacy scores (Table 3). The final index ranged from 0 to 6 and was subsequently classified into three microclimatic risk levels: low risk ($R \geq 5$), medium risk ($3 \leq R < 5$), and high risk ($R < 3$).

Table 3. Percentage contribution of variables to risk occurrence as a function of the microclimatic indicator.

Indicator	Contribution to High Risk	Contribution to Medium Risk	Contribution to Low Risk
Temperature	61.80%	7.93%	30.27%
Relative Humidity	65.11%	17.45%	17.44%
CO_2	63.13%	4.67%	32.20%

For this case study, the integration of these variables to obtain the final risk value based on the established rule base synthesized the overall behavior of the experiment. The results indicated that 63.08% of situations were related to high risk, while medium-risk conditions corresponded to 36.85% of the records.

Conversely, a percentage of 0.07% was found for the occurrence of low risk, demonstrating the rarity of simultaneously favorable conditions for all considered variables. This behavior shows that the environmental conditions observed in the semi-controlled chamber remained, for most of the time, outside the optimal ranges for soybean vegetative development according to the criteria adopted in this study.

3.5. Temporal Evolution of Risk During Vegetative Development

Temporal analysis of the integrated index revealed the dynamics of risk classes throughout the vegetative development of the crop. When applying the two analysis windows, the 3-day moving average captured transient environmental stress events, whereas the 5-day window indicated more persistent environmental conditions. Thus, a longer duration of unfavorable conditions within the analyzed windows increased the probability of physiological impacts on the crop. Table 4 presents the percentage distribution of the weighted behavior of the integrated risk according to each analytical time horizon.

Table 4. Percentage distribution of the combined microclimatic risk (R) index across the 3-day and 5-day temporal windows.

Temporal Window	High Risk	Medium Risk	Low Risk
Moving Average (3 days)	60.89%	38.95%	0.17%
Moving Average (5 days)	69.16%	30.68%	0.17%

The analysis of the temporal windows combined with the rule base illustrates a potential approach for studying plant behavior under the diverse risk situations that arise from the chosen climatic parameters (Figure 8). For this specific experiment, a higher incidence of high- and medium-risk windows was observed, which potentially compromised the productive development of the analyzed cultivar. In the 3-day moving average, high-risk conditions occurred during 60.89% of the experimental period. Expanding the analysis to the 5-day moving window, the percentage of records in high risk increased to 69.16%, while medium risk decreased to 30.68%.

On the other hand, the low-risk scenario remained identical in both moving windows at 0.17% occurrence, which statistically validates the rigor of the model. In general, despite the high percentage of high-risk situations, the plants found conditions to develop within the semi-protected environment during periods associated with the occurrence of medium- and low-risk.

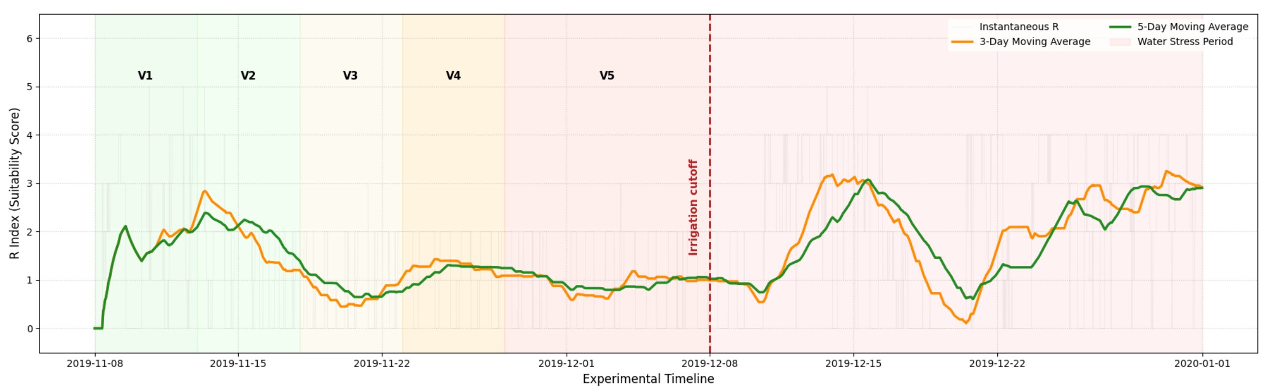

Fig. 8. Temporal evolution of the combined microclimatic risk (R) index and its respective moving averages (3 and 5 days) across soybean phenological stages.

In the initial phenological stages (V1 to V3), the integrated index exhibited trend toward medium-risk conditions according to the criteria adopted in this study. As the crop progressed to phenological stages V4 and V5, a stabilization of the moving average lines was observed around the high-risk trend level, with values close to 1. This behavior was associated with the increase in the physiological demand of the crop combined with air renewal limitations of the experimental environment, factors that directly influenced the dynamics of temperature, relative humidity, and CO_2 concentration.

Following the suspension of irrigation on December 8 (indicated by the vertical dashed line in Figure 8), the monitoring profile changed. In this case, cutting off irrigation eliminated the daily oscillations that varied within the high-risk trend. In the subsequent days (between December 8 and December 15), a temporary elevation of the trend curves toward low risk was observed. This behavior was driven by the breakdown of continuous humidity saturation in the chamber and a reduction in temperature values, temporarily altering the internal microclimatic balance.

However, this apparent improvement was interrupted around December 15; this trend suggests an intensification of microclimatic stress after prolonged periods without water replenishment. This decline reached its high-risk plateau (value equal to 0) near December 22, demonstrating the simultaneous hydrological and thermal collapse suffered by the plant, which occurred after the V5 phenological stage.

A subsequent rise in the index was observed at the end of the experimental period. This phenomenon, however, did not signify a physiological recovery of the plants, but rather reflected their collapse. With the advance of senescence, photosynthetic activity ceased. Due to the absence of daytime biotic consumption, the CO_2 concentration stabilized. Combined with the lack of humidity supersaturation and the drop in internal temperatures within the semi-controlled chamber—both resulting from the end of transpiration—the observed increase in the index did not represent an improvement in the physiological conditions of the crop, but rather an alteration of the microclimatic balance caused by the reduction in plant metabolic activity.

Thus, the temporal analysis of the risk index supported the decision-making process for identifying structural changes and their temporal variability within the microclimatic environment throughout the experimental cycle, highlighting periods of greater stability and intervals characterized by potentially limiting conditions for plant development.

4. Conclusion

This study successfully characterized a method for the temporal analysis of microclimatic variables and their influence on soybean crop development. The integration of sensors, Internet of Things (IoT) communication, time-series analysis, and multicriteria classification enabled the consolidation of a decision-support model applicable to Precision Agriculture. This framework proved fundamental for evaluating plant development dynamics in response to climatic oscillations within the monitored environment. The proposed risk index converted large volumes of environmental data into direct information regarding the stress level imposed on the crop. By synthesizing complex data into operational risk ranges, the model enhances agronomic interpretation. Consequently, the methodology provides robust support for monitoring systems aimed at increasing yield through guided management. Within protected environments, this approach assists in the early identification of critical periods and the validation of climate control strategies. The application of time-series analysis techniques—including Seasonal and Trend decomposition using Loess (STL) and moving averages—allowed for the identification of recurrent patterns, trends, and periods of greater microclimatic instability coupled with the phenological progress of soybean from stages V1 to V5. Additionally, the classification based on agronomic suitability ranges synthesized complex variables into a single, easily interpretable metric. The use of temporal windows proved strategic for distinguishing transient events from persistent trends, enabling an evolutionary assessment of risk throughout vegetative development and following the suspension of irrigation. From a Precision Agriculture perspective, the developed methodology extends beyond isolated temporal analysis. It establishes a continuous and scalable analytical baseline capable of integrating physical monitoring with biological plant responses, consolidating itself as a strategic tool for resource optimization and agricultural resilience against climatic vulnerabilities. Future research directions include the incorporation of physiological variables collected directly from the plant, which will further refine the predictive capacity and sensitivity of the proposed index.

Acknowledgments

The authors thank Embrapa Instrumentation, and the Pos-Graduation Program in Computer Science of the Federal University of São Carlos for the received support, as well as the project funded by the *Monsanto do Brasil* (Bayer Research Fund, linked to Phase I — Contract 35004.24/0070-7 - 21148.006747/2024-52).

5. References

Baker, J. T., Allen, L. H., Boote, K. J., Jones, P., & Jones, J. W. (1989). Response of soybean to air temperature and carbon dioxide concentration. *Crop Science, 29*(1), 98–105. https://doi.org/10.2135/cropsci1989.0011183x002900010024x

Embrapa Soja. (2026). *Dados econômicos: Soja em números (safra 2025/26).* Londrina, Brazil: Embrapa Soja. Available at: https://www.embrapa.br/soja/cultivos/soja1/dados-economicos. Last accessed 2 June 2026.

Embrapa. Centro Nacional de Pesquisa de Soja. (1991). *Cultivar de soja BR-16.* Londrina, Brazil: Embrapa Soja/SPSB.

Endres, G. J., & Kandel, H. (2025). *Soybean growth and management quick guide* (A1174, Revised June 2025). Fargo, USA: NDSU Extension Service.

Farias, J. R. B., Nepomuceno, A. L., & Neumaier, N. (2007). *Ecofisiologia da soja.* Londrina, Brazil: Embrapa Soja.

Fehr, W. R., & Caviness, C. E. (1977). *Stages of soybean development* (Special Report 80). Ames, USA: Iowa State University of Science and Technology.

He, Y., & Matthews, M. L. (2023). Seasonal climate conditions impact the effectiveness of improving photosynthesis to increase soybean yield. *Field Crops Research, 296*, 108907. https://doi.org/10.1016/j.fcr.2023.108907

Herrmann, P. S. P., Luccas, M. S., Ferreira, E. J., & Torre Neto, A. (2024). Application of electronic nose and machine learning used to detect soybean gases under water stress and variability throughout the daytime. *Frontiers in Plant Science, 15*, 1323296. https://doi.org/10.3389/fpls.2024.1323296

Jumrani, K., Bhatia, V. S., Kataria, S., & Landi, M. (2022). Screening soybean genotypes for high-temperature tolerance by maximin-minimax method based on yield potential and loss. *Agronomy, 12*(11), 2854. https://doi.org/10.3390/agronomy12112854

Kagan, C. R., et al. (2022). Special report: The internet of things for precision agriculture (IoT4Ag). *Computers and Electronics in Agriculture, 196*, 106742. https://doi.org/10.1016/j.compag.2022.106742

Kronenberg, L., et al. (2020). Rethinking temperature effects on leaf growth, gene expression and metabolism: Diel variation matters. *Plant, Cell & Environment, 44*(7), 2262–2276. https://doi.org/10.1111/pce.13958

Neumaier, N., Nepomuceno, A. L., Farias, J. R. B., & Oya, T. (2000). Estádios de desenvolvimento da cultura de soja. In E. R. Bonato (Ed.), *Estresses em soja* (pp. 19–43). Passo Fundo, Brazil: Embrapa Trigo.

Papa, R. A., Lacerda, M. P. C., Campos, P. M., Goedert, W. J., Ramos, M. L. G., & Kato, E. (2011). Qualidade de latossolos vermelhos e vermelho-amarelos sob vegetação nativa de cerrado. *Pesquisa Agropecuária Tropical, 41*(4), 564–571. https://doi.org/10.5216/pat.v41i4.13234

Silva, W. V. R., & Mann, R. (2023). Transformações na agricultura: Uma abordagem crítica sobre a agricultura de precisão. *IOSR Journal of Business and Management, 25*(12), 37–50.

Soares, J. C., Zimmermann, L., Santos, N. Z., Muller, O., Pintado, M., & Vasconcelos, M. W. (2021). Genotypic variation in the response of soybean to elevated CO_2. *Plant-Environment Interactions, 2*(6), 263–276. https://doi.org/10.1002/pei3.10065

United States Department of Agriculture. (2026). *World agricultural production.* Available at: https://www.fas.usda.gov/. Last accessed 22 April 2026.

Zhang, F., et al. (1995). Impact of low root temperatures in soybean [*Glycine max* (L.) Merr.] on nodulation and nitrogen fixation. *Environmental and Experimental Botany, 35*(3), 279–285. https://doi.org/10.1016/0098-8472(95)00017-7

Zou, D. S., & Kahnt, G. (1988). Effect of air humidity on photosynthesis and transpiration of soybean leaves. *Journal of Agronomy and Crop Science, 161*(3), 190–194. https://doi.org/10.1111/j.1439-037X.1988.tb00655.x